JCBFM Open

Journal of Cerebral Blood Flow & Metabolism (2012) 32, 1841–1852

www.jcbfm.com

Rapid Communication

Blood–spinal cord barrier pericyte reductions contribute to increased capillary permeability

Ethan A Winkler[1,2], Jesse D Sengillo[1], Robert D Bell[3], Joseph Wang[2] and Berislav V Zlokovic[1]

[1]*Department of Physiology and Biophysics, University of Southern California, Zilkha Neurogenetic Institute, Center for Neurodegeneration and Regeneration, Los Angeles, California, USA;* [2]*University of Rochester Medical Center, School of Medicine and Dentistry, Rochester, New York, USA;* [3]*University of Rochester Medical Center, Aab Cardiovascular Research Institute, Rochester, New York, USA*

The blood–spinal cord barrier (BSCB) regulates molecular exchange between blood and spinal cord. Pericytes are presumed to be important cellular constituents of the BSCB. However, the regional abundance and vascular functions of spinal cord pericytes have yet to be determined. Utilizing wild-type mice, we show that spinal cord pericyte capillary coverage and number compared with the brain regions are reduced most prominently in the anterior horn. Regional pericyte variations are highly correlated with: (1) increased capillary permeability to 350 Da, 40,000 Da, and 150,000 Da, but not 2,000,000 Da fluorescent vascular tracers in cervical, thoracic, and lumbar regions and (2) diminished endothelial zonula occludens-1 (ZO-1) and occludin tight junction protein expression. Pericyte-deficient mutations (*Pdgfrβ*$^{F7/F7}$ mice) resulted in additional pericyte reductions in spinal cord capillaries leading to overt BSCB disruption to serum proteins, accumulation in motor neurons of cytotoxic thrombin and fibrin and motor neuron loss. Barrier disruption in perciyte-deficient mice coincided with further reductions in ZO-1 and occludin. These data suggest that pericytes contribute to proper function of the BSCB at the capillary level. Regional reductions in spinal cord pericytes may provide a cellular basis for heightened spinal cord barrier capillary permeability and motor neuron loss.
Journal of Cerebral Blood Flow & Metabolism (2012) **32,** 1841–1852; doi:10.1038/jcbfm.2012.113; published online 1 August 2012

Keywords: blood–brain barrier; capillaries; endothelium; pericytes; vascular biology

Introduction

The blood–brain barrier (BBB) and blood–spinal cord barrier (BSCB) tightly regulate the blood–central nervous system (CNS) molecular exchange required for normal neuronal function (Zlokovic, 2008, 2011). In contrast to the highly permeable capillaries in the systemic circulation (Mann *et al*, 1985), blood–CNS vascular barriers are formed by continuous endothelial cells with tight junction protein complexes and low rates of vesicular transport (Winkler *et al*, 2011). This largely prohibits transport of large molecules and polar solutes without specific transport systems (Zlokovic and Apuzzo, 1997; Zlokovic, 2011). Although the BBB and BSCB are functionally similar, many differences have been identified (Bartanusz *et al*, 2011). For example, the rodent BSCB has heightened permeability to mannitol and inulin (Daniel *et al*, 1985; Prockop *et al*, 1995), interferons (Pan *et al*, 1997*a*), albumin, sucrose, and tumor necrosis factor α (Pan *et al*, 1997*b*). The source of these permeability changes is largely unknown, although reduced tight junction protein expression in the spinal cord has been reported (Ge and Pachter, 2006).

Pericytes are multifunctional members of the neurovascular unit (Armulik *et al*, 2011; Winkler *et al*, 2011). Pericytes ensheathe microvascular endothelial cells covering much of the vascular wall (Bell *et al*, 2012). Central nervous system pericytes have been demonstrated to promote development and maintenance of the BBB (Armulik *et al*, 2010; Bell *et al*, 2010; Daneman *et al*, 2010; Li *et al*, 2011), regulate capillary structure (Armulik *et al*, 2010; Bell *et al*, 2010; Enge *et al*, 2002; Hellstrom *et al*, 2001) and diameter (Armulik *et al*, 2010; Li *et al*, 2011;

Correspondence: Dr BV Zlokovic, Zilkha Neurogenetic Institute, Room: 301, 1501, San Pablo Street, Los Angeles, CA 90089, USA.
E-mail: berislav_zlokovic@urmc.rochester.edu
This research was supported by the ALS Association (Grant 1859) and the NIH Grant AG039452 to BVZ.
Received 23 May 2012; revised 3 July 2012; accepted 6 July 2012; published online 1 August 2012

Lindahl *et al*, 1997; Peppiatt *et al*, 2006), controversially, modulate capillary blood flow (Bell *et al*, 2010; Fernandez-Klett *et al*, 2010; Peppiatt *et al*, 2006), and participate in spinal cord scar formation (Goritz *et al*, 2011).

Although, pericytes are important cellular constituents of the BSCB (Bartanusz *et al*, 2011), their role in BSCB formation, maintenance and/or function is not known. Whether significant variations between brain and spinal cord pericyte populations exist and the functional consequences therein have been largely unexplored. In the present study, we analyzed pericyte populations and changes in barrier properties in multiple brain and spinal cord regions in mice under physiologic conditions and in pericyte-deficient mice.

Materials and methods

Animals

All experimental protocols and animal handling procedures were performed in accordance with the National Institutes of Health (NIH, USA) guidelines for the use of experimental animals and the experimental protocols were approved by the Institutional Animal Care and Use Committee at the University of Southern California. Adult 2-month-old male B6SJLF1/J mice devoid of CNS neuropathology were purchased from Jackson Laboratories (Bar Harbor, ME, USA). Adult male 4- to 6-month-old pericyte-deficient $Pdgfr\beta^{F7/F7}$ mice on a 129S1/SvlmJ background were generated and maintained as described (Tallquist *et al*, 2003). Adult 4- to 6-month-old nontransgenic 129S1/SvlmJ littermates were used as controls for $Pdgfr\beta^{F7/F7}$ mice. Adult 13-month-old $Pdgfr\beta^{F7/F7}$ mice and 13-month-old nontransgenic 129S1/SvlmJ littermates were utilized for neuronal analysis.

Tissue Preparation

Animals were anesthetized with intraperitoneal injection of 100 mg/kg ketamine and 10 mg/kg xylazine and transcardially perfused with phosphate-buffered saline (PBS) containing 5 mM EDTA (Sigma-Aldrich, St Louis, MO, USA). In a separate set of studies, mice were intravenously injected with 0.1 mL of Alexa Fluor 546-conjugated cadaverine diluted 0.5 μg/μL. Cadaverine was allowed to circulate for 2 hours and then mice were transcardially perfused. The brains were excised from the skull and prepared for subsequent analysis. For spinal cord isolation, mice were decapitated and the vertebral column was dissected. An 18-gauge needle attached to a 3-mL syringe was placed in the sacral opening of the vertebral column and the intact spinal cord was discharged with cold PBS. Once isolated, the brain and spinal cords were either prepared for microvessel isolation (see below), immersion fixed in 4% PFA (paraformaldehyde) (Sigma-Aldrich) overnight at 4°C, or embedded in optimal cutting temperature compound (Tissue-Tek, Torrance, CA, USA). Fixed tissues were sectioned at a thickness of 40 μm with a Leica VT1000S vibrating blade microtome (Leica Instruments, Nussloch, Germany) in preparation for immunofluorescent analysis. Tissues embedded in optimal cutting temperature were cryosectioned at a thickness of 14 μm and subsequently fixed in ice-cold acetone in preparation for immunofluorescent analysis.

Microvessel Isolation

Following tissue removal, microvessels were isolated as we previously described for the brain (Bell *et al*, 2010; Zlokovic *et al*, 1993, 2000) and spinal cord (Zhong *et al*, 2008, 2009). Meninges and large pial vessels were carefully removed and regions of interest including cortex, caudate, hippocampus, cervical, thoracic, and lumbar spinal cord were isolated under a dissecting microscope. White matter was excised and discarded from each region. The spinal cord was bisected and only anterior portions were used for isolation. Identical regions from five individual mice were pooled to maximize yield from each preparation. Tissue was then cut into small pieces with a scalpel (~1 to 2 mm in size) and homogenized in a Dounce homogenizer containing PBS with 2% FBS (fetal bovine serum) (Invitrogen, Carlsbad, CA, USA). Homogenate was centrifuged at 6000 *g* for 20 minutes in 18% dextran solution (MW: ~70,000 Da; Sigma-Aldrich) in PBS containing 2% FBS. Following centrifugation, floating glial and neuronal elements were gently aspirated and the vascular pellet was resuspended in PBS containing 2% FBS. Isolated microvessels were then passed through a 100-μm cell strainer to remove larger vessels and debris. Flow through was collected and then passed through a 40-μm cell strainer to remove red blood cells. Microvessels were trapped on top of cell strainer, which was subsequently inverted and rinsed to collect microvessels in 50 mL conical tube. A small aliquot was visualized at ×10 magnification with a standard light microscope to confirm purity and yield. Microvessel preparations from each region were adhered to glass histology slides using a Cytospin III Cytocentrifuge (Shandon, Pittsburgh, PA, USA) and fixed in 4% PFA for 20 minutes for immunofluorescent analysis. Three independent preparations were utilized for all studies (15 mice in total).

Immunofluorescent and Fluorescent Analysis

Free-floating 40 μm thick PFA-fixed coronal brain and spinal cord sections were initially blocked and permeabilized with 10% swine serum (Vector Laboratories, Burlingame, CA, USA) containing 0.1% Triton X-100 (Sigma-Aldrich). Sections were then incubated in the following primary antibodies: goat α-mouse CD13 (10 μg/mL; R&D Systems, Minneapolis, MN, USA), goat α-mouse platelet-derived growth factor receptor β (PDGFRβ) (10 μg/mL; R&D Systems), mouse α-mouse neuronal-specific antigen A60 (NeuN) (1:100, EMD Millipore, Billerica, MA, USA) or rabbit α-mouse collagen IV (1:200, EMD Millipore). To visualize pericytes, sections were then incubated in bovine anti-goat Cy3 (Jackson ImmunoResearch Laboratories, West Grove, PA, USA) diluted 1:100 to detect CD13 or PDGFRβ. To visualize endothelial cells, sections were incubated in

either donkey anti-rabbit Alexa Fluor 488 (Jackson ImmunoResearch) diluted 1:100 to detect collagen IV or biotin-labeled *Lycoperiscon esculentum* (tomato) lectin (Vector Labs) diluted 1:100. Sections treated with lectin were then incubated in Dylight 649-conjugated streptavidin (Vector Labs) to detect endothelial-specific fluorescent signal. Nuclei were detected with Hoechst 33342 (Invitrogen) diluted 1:10,000.

In a separate set of studies, 14 μm thick acetone fixed coronal spinal cord sections were blocked with 10% swine serum. Sections were then incubated in the following primary antibodies: goat α-mouse CD13 (10 μg/mL, R&D Systems), mouse α-mouse desmin (1:100, Dako, Carpinteria, CA, USA), rabbit α-mouse collagen IV (1:200, EMD Millipore), rabbit α-human fibrin which cross reacts with mouse fibrin (1:500, Dako), goat α-mouse thrombin (1:50, Santa Cruz Biotechnology, Santa Cruz, CA, USA), mouse α-mouse zonula occludens-1 (ZO-1) (1:50, Invitrogen), mouse α-mouse occludin (1:50, Invitrogen), mouse α-mouse neuronal-specific antigen A60 (NeuN) (1:100, EMD Millipore) and goat anti-mouse ChAT (choline acetyl transferase) (1:50, EMD Millipore). To visualize pericytes, sections were incubated in bovine anti-goat Cy3 or donkey anti-mouse Cy3 (Jackson ImmunoResearch Laboratories) diluted 1:100 to detect CD13 or desmin, respectively. To visualize plasma proteins, sections were incubated with donkey anti-rabbit Cy3 or bovine anti-goat Alexa Fluor 488 (Jackson ImmunoResearch) diluted 1:100 to visualize fibrin and thrombin, respectively. To visualize tight junction proteins, sections were incubated in donkey anti-mouse Alexa Fluor 488 (Jackson ImmunoResearch) diluted 1:100 to visualize occludin and ZO-1 and for collagen IV-positive endothelial cells in donkey anti-rabbit Cy3, Alexa Fluor 488 or DyLight 649. To visualize motor neurons, sections were incubated with donkey anti-mouse Alexa Fluor 488 (Jackson ImmunoResearch) and bovine anti-goat Cy3 (Jackson ImmunoResearch) diluted 1:100 to detect NeuN and ChAT, respectively.

In a separate set of studies, PFA-fixed microvessel preparations were blocked and permeabilized with 10% swine serum containing 0.05% Triton X-100. Microvessels were then incubated in the following primary antibodies: mouse α-mouse ZO-1 (1:50, Invitrogen), rabbit α-mouse occludin (1:100, Invitrogen) or rabbit α-mouse claudin-5 (1:200, Millipore). To visualize tight junctions, microvessels were incubated in donkey anti-mouse Alexa Fluor 488 (Jackson ImmunoResearch) or donkey anti-rabbit Alexa Fluor 488 (Jackson ImmunoResearch) to detect ZO-1 or occludin and claudin-5, respectively. To visualize endothelial cells, sections were incubated in DyLight 594-conjugated *L. esculentum* (tomato) lectin (Vector Labs) diluted 1:100.

Tissue sections and microvessel preparations were mounted with fluorescent mounting media (Dako) and coverslipped. All slides were scanned with a custom built Zeiss 510 meta confocal laser scanning microscope with a Zeiss Apochromat $\times$ 25/0.8 NA water immersion objective (Car Zeiss Microimaging, Thornwood, NY, USA). A 488-nm argon laser was used to excite Alexa Fluor 488 and the emission was collected through a 500 to 550 nm band pass (bp) filter. A 543-nm HeNe laser was used to excite Cy3, Alexa Fluor 546 and DyLight 549 and the emission was collected through a 560 to 615 nm bp filter. A 633-nm HeNe laser was used to excite DyLight 649 and the emission was collected through a 650 to 700 nm bp filter. A 800-nm tuned Ti:sapphire laser (Specra Physics, Irvine, CA, USA) was used to excite Hoechst 33342 and the emission was collected through a 435 to 485 bp filter.

Image Analysis

All image analysis was conducted utilizing NIH ImageJ software. All image analyses were performed by a blinded investigator. For pericyte coverage analysis, CD13-, PDGFRβ-, or desmin-positive surface area was determined by the ImageJ Area measurement tool and divided by the lectin- or collagen IV-positive capillary surface area, respectively, as we previously described (Bell *et al*, 2010). For pericyte number analysis, PDGFRβ- or CD13-positive perivascular cell bodies located on the abluminal endothelial cell wall that co-localized with Hoechst-positive nuclei were counted using the ImageJ Cell Counter plug-in and expressed per mm^2 lectin- or collagen IV-positive capillary surface area, respectively, as previously reported (Bell *et al*, 2010; Pfister *et al*, 2008). For tight junction protein analysis, ZO-1-, occludin- or claudin-5-positive immunofluorescent length was determined by the ImageJ Length measurement tool divided by the lectin-positive capillary surface area as we previously described (Bell *et al*, 2010). Values were expressed as mm tight junction length per mm^2 capillary surface area. For motor neuron analysis, NeuN- and ChAT-positive cells were manually counted in the anterior horn of the lumbar spinal cord in six nonadjacent sections ($\sim$100 μm apart) and expressed as motor neurons per lumbar section as previously described (Jaarsma *et al*, 2008).

For all analyses, a field size of 420 $\times$ 420 μm^2 was utilized and 10 to 12 μm maximum projection *z*-stack images were reconstructed. For all studies examining region variability, three randomly selected fields per section from three nonadjacent sections ($\sim$100 μm apart) were analyzed. Six mice were analyzed per region. For studies utilizing *Pdgfr*$\beta^{+/+}$ and *Pdgfr*$\beta^{F7/F7}$ mice, three randomly selected fields per section from three nonadjacent sections ($\sim$100 μm apart) were analyzed. Three to four mice were analyzed per region. For studies utilizing isolated microvessels, a minimum of five randomly selected 420 $\times$ 420 μm^2 fields were selected per preparation (five mice per preparation). Three to four independent preparations were utilized per parameter.

Noninvasive Fluorometric Permeability Studies

Regional BBB and BSCB permeability to fluorescent tracers of different molecular weights including tetramethylrhodamine (TMR)-dextran (40,000 Da; Invitrogen), TMR-dextran (150,000 Da; Invitrogen) and Fluorescein-mega-dextan (MW: 2,000,000) were determined as we previously described (Bell *et al*, 2010). Dextrans of multiple molecular weights were individually diluted to a final concentration of 10 mg/mL and injected via the femoral vein at a volume of 0.1 mL. Orbital sinus blood samples were collected before injection and 2, 10, 15, 20, and 30 minutes postinjection. Following

30 minutes of fluorescent tracer circulation, animals were transcardially perfused with PBS containing 5 mM EDTA to remove residual tracer confined within the brain and spinal cord vasculature. Cortex, caudate, hippocampus, cervical, thoracic, and lumbar spinal cord regions were separately dissected. Tissues from each CNS region were individually weighed, homogenized in 10 volumes of 1% Triton X-100 (Sigma-Aldrich), and centrifuged to obtain a supernatant for analysis. Plasma samples were diluted (1:25 to 1:100) and 100 μL of plasma samples and brain homogenates (undiluted) were then analyzed using a Victor fluorometric plate reader (Perkin-Elmer, Waltham, MA, USA). A wavelength of 543 nm and 488 nm was used for excitation and emission was collected at 590 nm and 535 nm for TMR and Fluorescein, respectively.

Calculation of Permeability-Surface Area (PS) Product from Fluorometric Permeability Studies

The PS product (mL per gram per minute) was determined for each tracer in each CNS region by dividing the brain fluorescent intensity values by the integrated plasma fluorescent intensity value over 30 minutes of tracer circulation. The PS product was calculated using equation (1) as we previously described (Mackic *et al*, 1998).

$$PS = C_b/({}_0\int^T C_p x T). \quad (1)$$

Where C_b and ${}_0\int^T C_p$ are defined as the fluorescent tracer concentration in the brain (per gram tissue) and integrated plasma concentration, respectively, and T represents experimental time.

Statistical Analysis

All data were analyzed using multifactorial analysis of variance (ANOVA) followed by Tukey *posthoc* tests. Correlations were determined using Pearson's correlation analysis. A P value <0.05 was considered statistically significant in all studies.

Results

Blood–Spinal Cord Barrier Pericyte Coverage and Number Are Reduced in Comparison to Brain

Pericytes represent a heterogenous cell population not covered by a single cell marker that is specific or inclusive (Armulik *et al*, 2011; Winkler *et al*, 2011). Therefore, both, Aminopeptidase-N (CD13) (Armulik *et al*, 2010) and PDGFRβ (Bell *et al*, 2010; Daneman *et al*, 2010; Lindahl *et al*, 1997; Winkler *et al*, 2010) previously established to be abundantly expressed in CNS pericytes were independently analyzed to determine CNS pericyte populations. Consistent with previous reports, quantification of the percentage of the capillary wall covered by pericyte cell processes positive for CD13 (Figures 1A and 1B) or PDGFRβ (Figures 1D and 1E) in the brain regions was $\sim$80% (Armulik *et al*, 2010; Bell *et al*, 2010; Daneman *et al*, 2010; Li *et al*, 2011) and did not vary in cortex, caudate, and/or hippocampus (Bell *et al*, 2010). In contrast, CD13-positive and PDGFRβ-positive pericyte coverages were significantly reduced in cervical, thoracic, and lumbar spinal cord anterior horn capillaries covering only 59% to 55%, 68% to 66%, and 52% to 48% of the endothelial cell wall, respectively (Figures 1A, 1B, 1D, and 1E). Next, using previously published methods (Armulik *et al*, 2010; Bell *et al*, 2010; Pfister *et al*, 2008), we evaluated whether there were similar reductions in pericyte number that may contribute to the observed reductions in capillary coverage. Counting CD13-positive (Figure 1C) or PDGFRβ-positive (Figure 1F) pericytes per mm^2 capillary area revealed $\sim$47% to 45%, 28% to 33%, and 49% to 53% reductions in cervical, thoracic, and lumbar anterior horn pericyte number, respectively, when compared with the brain regions.

Pericyte coverage and/or populations were not uniformly reduced within the spinal cord regions. For example, CD13-positive pericyte capillary coverage was much higher in cervical, thoracic, and lumbar white matter funiculi as evidenced by capillary coverage values of 68%, 75%, and 68%, respectively (Figures 2A and 2B). Platelet-derived growth factor receptor β-positive pericyte processes showed similarly higher white matter capillary coverage values of 73%, 73%, and 68% in cervical, thoracic, and lumbar funiculi (Figure 2D). CD13- (Figure 2C) and PDGFRβ-positive (Figure 2E) pericyte numbers per mm^2 capillary area were significantly higher in white matter regions when compared with gray matter. These data suggest that BSCB pericyte reductions are most pronounced in the spinal cord regions enriched with neuronal cell bodies.

Reduced Pericyte Coverage is Correlated with Increased Blood–Spinal Cord Barrier Permeability

To determine regional BBB and BSCB permeability in wild-type mice, we first injected the fluorescently conjugated vascular tracer cadaverine (MW: 350 Da). In vessels with tight barrier properties, such as the BBB, no residual tissue and/or intravascular fluorescent signal was observed following perfusion (Figure 3A). In contrast, increased parenchymal fluorescence greatest in anterior horn regions were detected in cervical, thoracic, and lumbar spinal cord following perfusion, suggesting heightened barrier tracer flux (Figure 3A). Importantly, no significant differences in tissue autofluorescence were detected between brain and spinal cord as evidenced by the noninjected control (Figure 3A). Spinal cord accumulation of 40,000 Da and 150,000 Da dextans was not detected by microscopy (data not shown).

To quantify the magnitude of vascular leakage and determine the molecular cutoff and size specificity of regional BSCB permeability changes, we next injected individual fluorescently labeled dextrans of different molecular weights and utilized a more

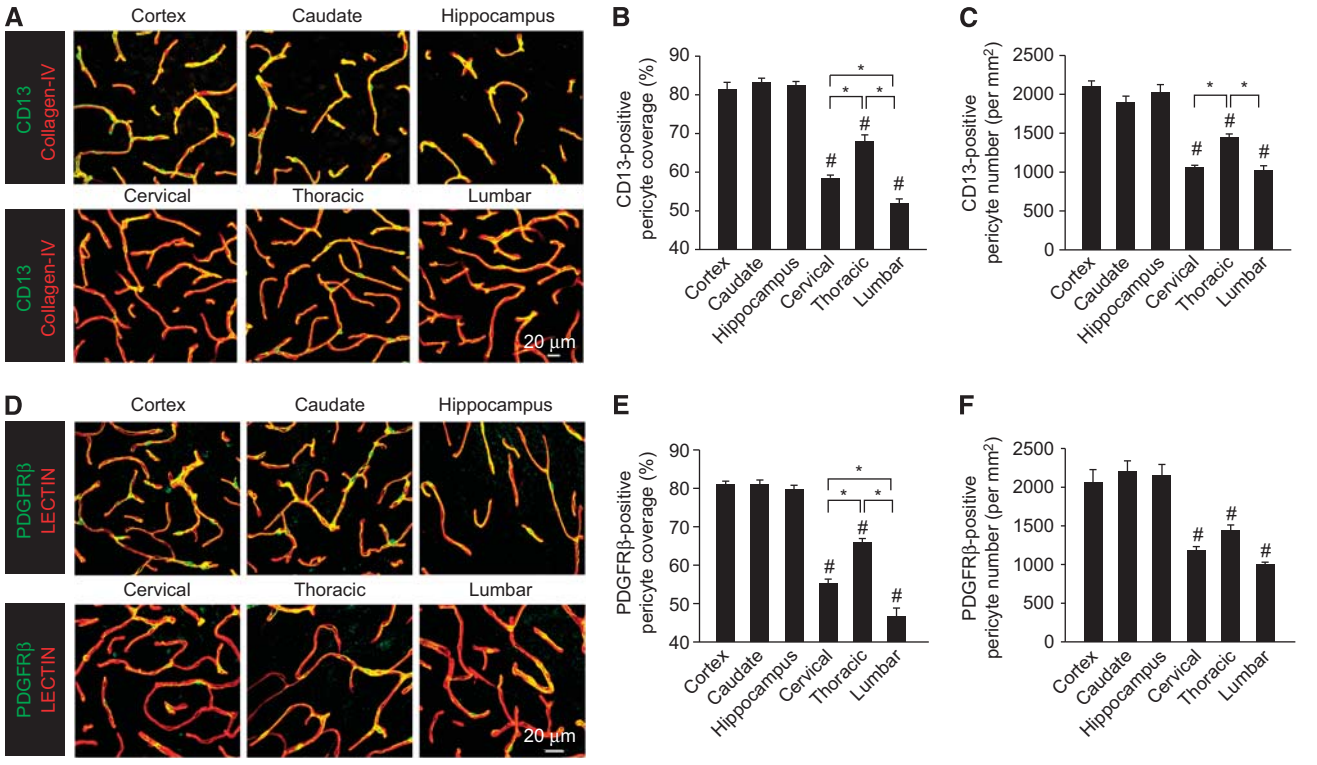

Figure 1 Pericyte number and coverage is reduced along blood–spinal cord barrier. (**A**) Confocal microscopy analysis of CD13-positive pericytes (green) and collagen IV-positive capillary profiles (red) in 2-month-old wild-type mouse cortex, caudate, and hippocampal brain regions and cervical, thoracic, and lumbar spinal cord regions (anterior horns). (**B**) Quantification of regional CD13-positive pericyte coverage of collagen IV-positive brain and spinal cord capillaries. Mean ± s.e.m., $n = 5$ to 7 animals per group. $^{\#}P < 0.05$ when compared with the brain regions; $^{*}P < 0.05$. (**C**) Quantification of regional CD13-positive pericyte cell number normalized to collagen IV-positive capillary surface area in the brain and spinal cord. Mean ± s.e.m., $n = 5$ to 7 animals per group. $^{\#}P < 0.05$ when compared with the brain regions; $^{*}P < 0.05$. (**D**) Confocal microscopy analysis of platelet-derived growth factor receptor β (PDGFRβ)-positive pericytes (green) and lectin capillary profiles (red) in 2-month-old wild-type mouse cortex, caudate, and hippocampal brain regions and cervical, thoracic, and lumbar spinal cord regions. (**E**) Quantification of regional PDGFRβ-positive pericyte coverage of lectin-positive brain and spinal cord capillaries. Mean ± s.e.m., $n = 7$ animals per group. $^{\#}P < 0.05$ when compared with the brain regions; $^{*}P < 0.05$. (**F**) Quantification of regional PDGFRβ-positive pericyte cell number normalized to lectin-positive capillary surface area in the brain and spinal cord. Mean ± s.e.m., $n = 7$ animals per group. $\#P < 0.05$ when compared with the brain regions; $^{*}P < 0.05$.

sensitive assay to measure residual tissue fluorescence following perfusion as previously established (Bell *et al*, 2010). Analysis revealed ~3.8-, 3.1-, and 4.3-fold increases in barrier permeability to 40,000 Da dextran in cervical, thoracic, and lumbar spinal cords, respectively, when compared with the brain regions (Figure 3B). Blood–spinal cord barrier permeability to 150,000 Da was also increased, albeit to a lesser degree, as evidenced by 2.3-, 1.5-, and 2.6-fold increases in PS product in cervical, thoracic, and lumbar spinal cord (Figure 3C). In contrast, there was no detectable leakage of mega-dextran (2,000,000 Da), indicating barely detectable values in all spinal cord and/or brain regions (Figure 3C). Importantly, heightened BSCB permeability to both 40,000 Da (Figure 3D) and 150,000 Da (Figure 3E) showed a significant negative correlation with regional pericyte capillary coverage, suggesting that regional pericyte coverage reductions in the spinal cord are associated with permeability changes.

Increased Blood–Spinal Cord Barrier Barrier Permeability is Associated with Reduced Tight Junction Protein Expression

Pericyte reductions have been previously associated with reduced tight junction protein expression and misalignment (Bell *et al*, 2010; Daneman *et al*, 2010). To evaluate tight junctional proteins, we next measured endothelial ZO-1, occludin, and claudin-5 tight junctional length in the brain and spinal cord capillaries. Tight junctional length measurements for ZO-1, an important adaptor protein linking transmembrane junctional complexes to the underlying actin cytoskeleton (Zlokovic, 2008, 2011), revealed ~42%, 37%, and 47% reductions in cervical, thoracic, and lumbar spinal cord capillaries, respectively, when compared with the brain regions (Figures 4A and 4B). Similar analysis revealed even greater 62%, 37%, and 65% reductions in the transmembrane tight junctional protein occludin complexes in cervical, thoracic, and lumbar capillaries, respectively (Figures 4C and 4D).

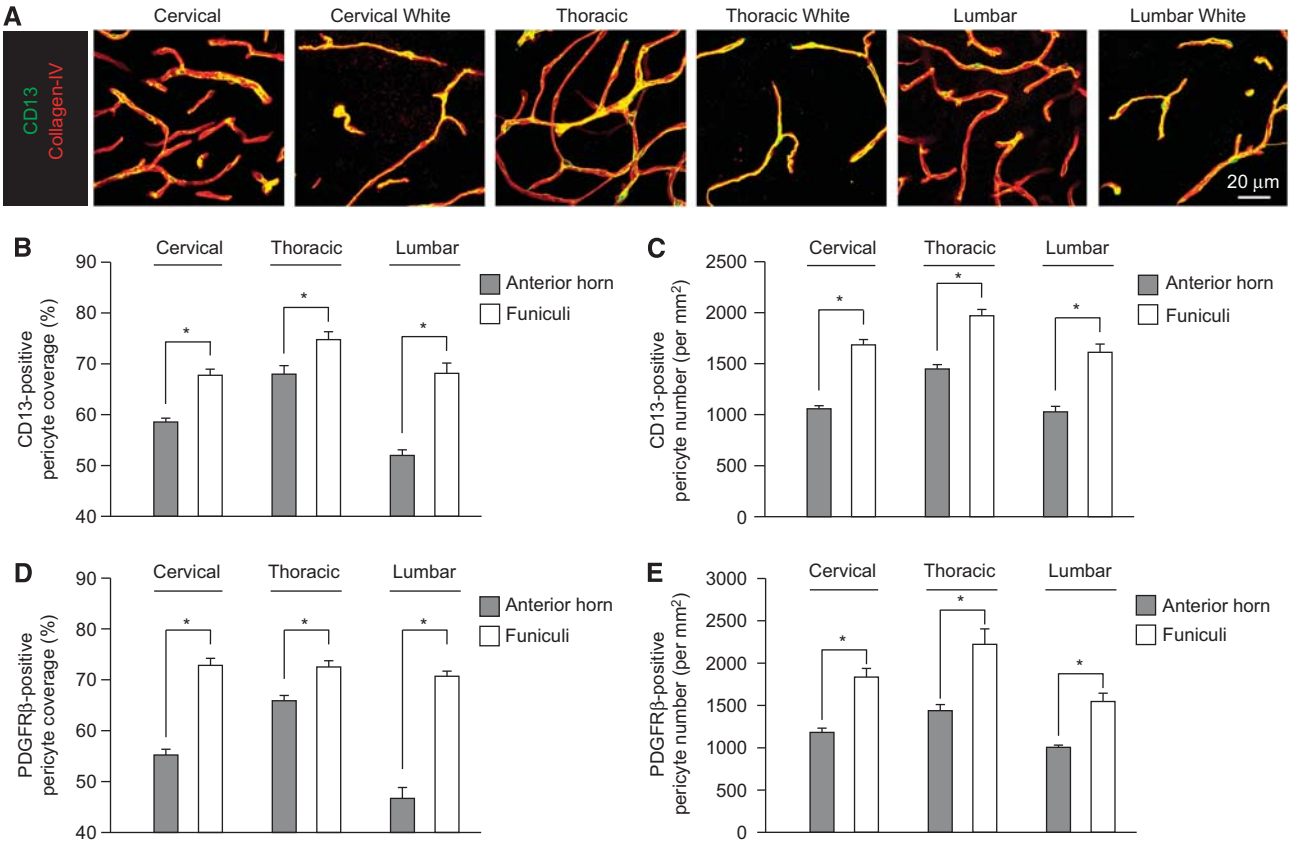

Figure 2 Subregional variation in spinal cord pericyte number and coverage between anterior horn gray matter and lateral and dorsal funiculi. (**A**) Confocal microscopy analysis of CD13-positive pericytes (green) and collagen IV-positive capillary profiles (red) in 2-month-old wild-type mouse anterior horn gray matter or dorsal columns for cervical thoracic and lumbar spinal cord. (**B**) Quantification of CD13-positive pericyte coverage of collagen IV-positive capillaries in anterior horn gray matter (gray) or dorsal and lateral funiculi (white) from cervical, thoracic, and lumbar spinal cord. Mean ± s.e.m., $n = 5$ to 7 animals per group; $^*P < 0.05$. (**C**) Quantification of CD13-positive pericyte cell number normalized to lectin-positive capillary surface area in anterior horn gray matter (gray) or dorsal and lateral funiculi (white) from cervical, thoracic, and lumbar spinal cord. Mean ± s.e.m., $n = 5$ to 7 animals per group; $^*P < 0.05$. (**D**) Quantification of platelet-derived growth factor receptor β (PDGFRβ)-positive pericyte coverage of lectin-positive capillaries in anterior horn gray matter (gray) or dorsal and lateral funiculi (white) from cervical, thoracic, and lumbar spinal cord. Mean ± s.e.m., $n = 7$ animals per group; $^*P < 0.05$. (**E**) Quantification of PDGFRβ-positive pericyte cell number normalized to lectin-positive capillary surface area in anterior horn gray matter (gray) or dorsal and lateral funiculi (white) from cervical, thoracic, and lumbar spinal cord. Mean ± s.e.m., $n = 7$ animals per group; $^*P < 0.05$.

Consistent with a previous report (Ge and Pachter, 2006), no significant changes in the transmembrane tight junctional protein claudin-5 were detected in the spinal cord and brain capillaries (Figures 4E and 4F). Together, these data suggest that BSCB permeability increases might arise from increased paracellular flow through diminished tight junctional protein complexes in BSCB regions with reduced pericyte coverage.

Pericyte Deficiency Exacerbates Spinal Cord Capillary Leakage and Tight Junctional Abnormalities

To more directly study the roles of pericytes in BSCB function, we next analyzed permeability and structural changes in well-characterized pericyte-deficient *Pdgfrβ*$^{F7/F7}$ mice (Bell *et al*, 2010; Tallquist *et al*, 2003). Quantitative immunofluorescent analysis revealed 39%, 39%, and 43% reductions in CD13-positive pericyte capillary coverage in cervical, thoracic, and lumbar spinal cord capillaries, respectively (Figures 5A and 5B). Similar 40%, 35%, and 43% reductions in desmin-positive pericyte capillary coverage were observed in cervical, thoracic, and lumbar spinal cord (data not shown), thereby confirming that BSCB pericyte populations are further reduced in *Pdgfrβ*$^{F7/F7}$ mutants and may serve as a valuable model to deduce BSCB pericyte function.

We next evaluated whether BSCB pericyte deficiency directly exacerbates capillary leakage and motor neuron accumulation of the endogenous plasma proteins IgG and Fibrin (Figure 5C). Quantification of extravascular IgG (MW: 150,000 Da) and fibrin (MW: 53,000 to 73,000 Da) demonstrated significant increases in spinal cord accumulation in

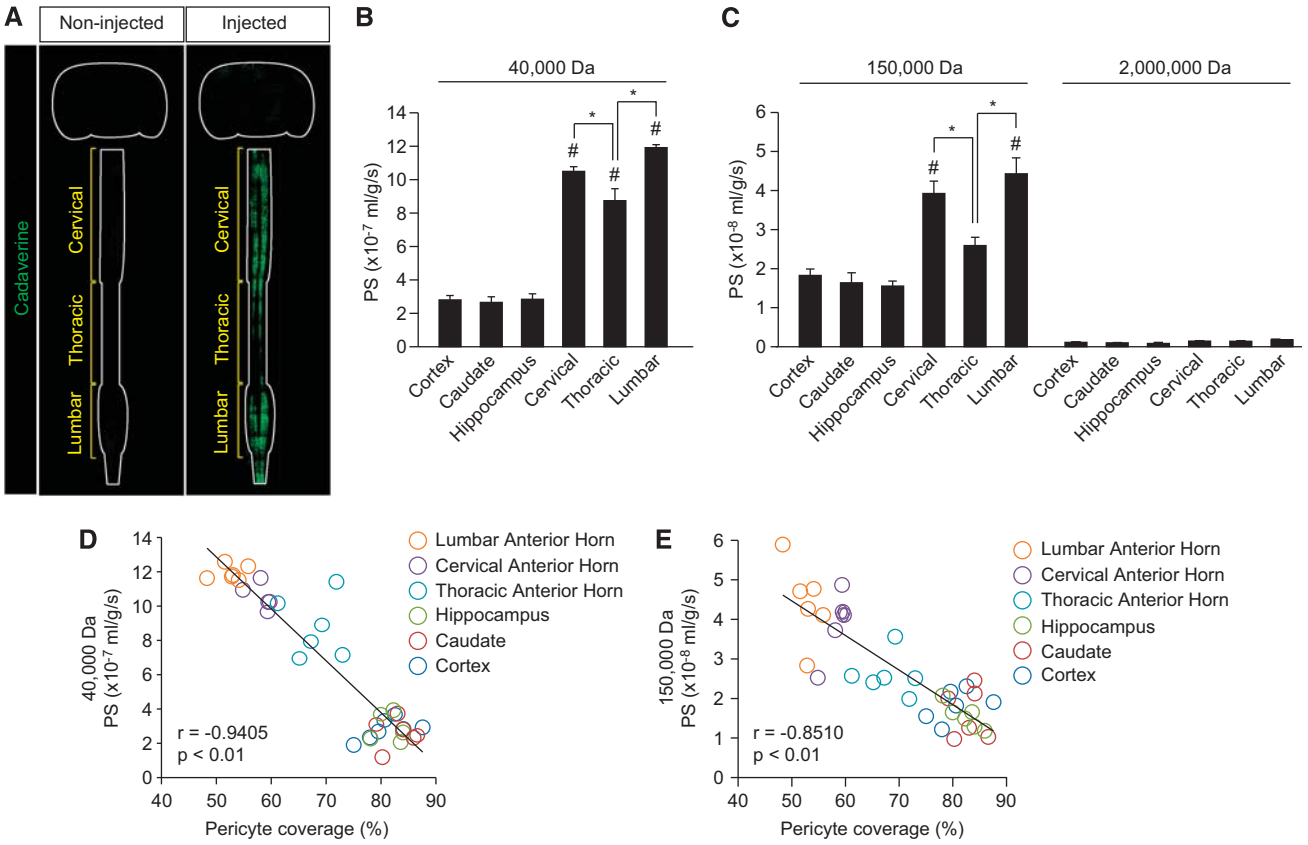

Figure 3 Heightened blood–spinal cord barrier (BSCB) permeability is highly correlated with regional reductions in pericyte coverage. (**A**) Regional fluorescent detection of intravascularly administered cadaverine (green) in 2-month-old wild-type spinal cord (longitudinal section, but not brain coronal section). Broken line represents outline of tissue section. Left, noninjection control; Right, injected mouse. (**B**, **C**) Blood–brain barrier (BBB) and BSCB permeability PS products for tetramethylrhodamine (TMR)-dextran (40,000 Da) (**B**) and TMR-dextran (150,000 Da) and fluorescein conjugated-mega-dextran (2,000,000 Da) (**C**) in 2-month-old mouse cortex, caudate, hippocampus, cervical, thoracic, and lumbar spinal cord. Mean ± s.e.m., $n = 6$ mice per group for TMR-dextran, $n = 3$ mice per group for mega-dextran. $^{\#}P < 0.05$ when compared with the brain regions; $^{*}P < 0.05$. (**D**, **E**) Negative correlation between the PS products for TMR-dextran (40,000 Da) (**D**) and TMR-dextran (150,000 Da) (**E**) and regional pericyte capillary coverage in 2-month-old wild-type mice. *r*, Pearson's coefficient.

cervical, thoracic, and lumbar regions of *Pdgfrβ*$^{F7/F7}$ mice (Figures 5D and 5E). No strain-specific differences in deposition of plasma-derived IgG (Figure 5D) or fibrin (Figure 5E) were detected between nontransgenic mouse lines. Increased spinal barrier disruption led to neuronal accumulation of several potentially neurotoxic plasma proteins including thrombin (MW: 36,000 Da) (Figure 5F) and fibrin (Figure 5G) in lumbar spinal cord of *Pdgfrβ*$^{F7/F7}$ mice. Similar results were obtained in cervical and thoracic spinal cord (data not shown). In contrast, plasma proteins were not seen to accumulate in the spinal cord of nontransgenic mice (Figures 5F and 5G). These data suggest that increased BSCB disruption caused by an additional pericyte loss in *Pdgfrβ*$^{F7/F7}$ mice is required to render motor neurons vulnerable to accumulation of larger molecular weight and potentially harmful plasma proteins.

To further deduce whether pericyte-associated BSCB permeability deficits were paracellular in character, we utilized similar immunofluorescent analysis of tight junctional complexes in *Pdgfrβ*$^{F7/F7}$ mice as we did in nontransgenic mice. Analysis of ZO-1 tight junctional length revealed further 26%, 21%, and 30% reductions in junctional length in the anterior horn of cervical, thoracic, and lumbar spinal cord from *Pdgfrβ*$^{F7/F7}$mice when compared with age-matched nontransgenic mice (Figures 6A and 6B). Similar analysis revealed 34%, 39%, and 51% reductions in occludin (Figures 6C and 6D) junctional length in anterior horn cervical, thoracic, and lumbar *Pdgfrβ*$^{F7/F7}$ mouse spinal cord. No strain-specific differences were detected in ZO-1 (Figure 6B) or occludin (Figure 6D) tight junctional length between nontransgenic mouse lines.

Pericyte Deficiency Contributes to Motor Neuron Loss in the Spinal Cord

Previously, pericyte reduction and/or dysfunction and plasma protein leakage has been shown to

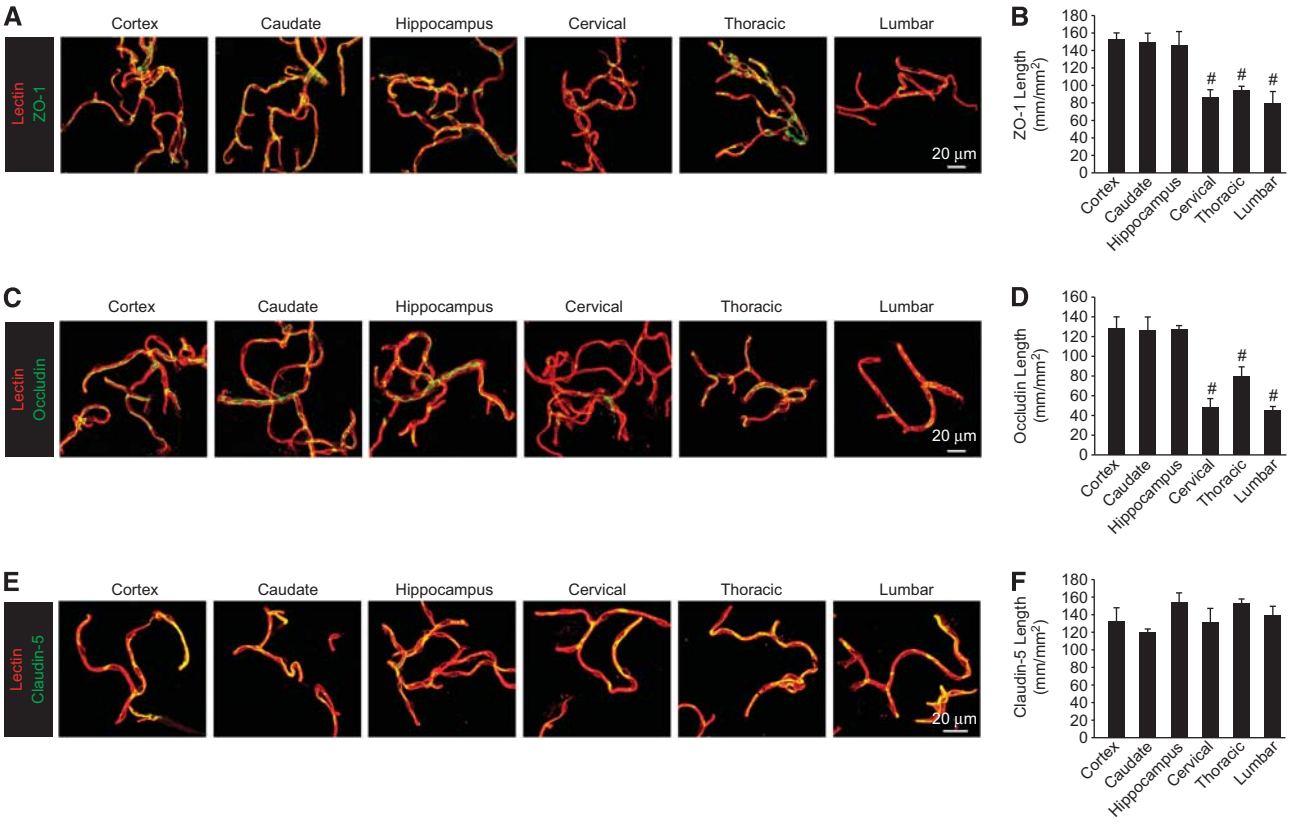

Figure 4 Reduced pericyte coverage along blood–spinal cord barrier is associated with reduced tight junction protein expression. (**A**, **C**, **E**) Confocal microscopy analysis of tight junction zonula occludens-1 (ZO-1) (**A**), occludin (**C**), or claudin-5 (**E**) immunodetection (green) in acutely isolated lectin-positive capillaries (red) from 2-month-old mouse cortex, caudate, hippocampus, cervical, thoracic, and lumbar spinal cord. (**B**, **D**, **F**) Quantification of endothelial ZO-1 (**B**), occludin (**D**), or claudin-5 (**F**) tight junctional length in acutely isolated vessel preparations from the brain and spinal cord regions. Mean ± s.e.m. $n = 3$ to 4 preparations per group (five mice per preparation); $^{\#}P < 0.05$ when compared with the brain regions.

contribute to neurodegenerative changes in the brain (Bell *et al*, 2010, 2012; Winkler *et al*, 2011). To deduce whether similar changes may contribute to motor neuron injury in the spinal cord, we first analyzed gross structural changes in the lumbar spinal cord of 13-month-old $Pdgfr\beta^{F7/F7}$ mice and age-matched nontransgenic littermates. Bright-field microscopy analysis demonstrated reduced cellularity, especially in large cells morphologically consistent with motor neurons, in the lumbar spinal cord anterior horn of $Pdgfr\beta^{F7/F7}$ mice when compared with nontransgenic littermates (Figure 7A). To confirm motor neuron loss, we utilized an established technique to quantitate motor neurons (Jaarsma *et al*, 2008). Analysis revealed approximately a 19% reduction in the number of motor neurons in the lumbar spinal cord anterior horn in $Pdgfr\beta^{F7/F7}$mice when compared with nontransgenic littermates (Figures 7B and 7C).

Discussion

Our findings suggest that as in the brain (Armulik *et al*, 2010; Bell *et al*, 2010; Daneman *et al*, 2010; Li *et al*, 2011) and retina (Kim *et al*, 2009), pericytes contribute to vascular barrier properties in the spinal cord. Unlike the relative uniformity of pericyte capillary coverage and cell number in the brain regions (Bell *et al*, 2010), pericyte coverage and number are reduced in anterior horn spinal cord capillaries in wild-type mice. Consistent with previous reports (Daniel *et al*, 1985; Pan *et al*, 1997*a*, *b*; Prockop *et al*, 1995), we found increased spinal cord capillary permeability most pronounced in the cervical and lumbar regions to multiple tracers $\leq$150,000 Da, which correlated with reductions in pericyte coverage. The present study also shows that deficient PDGFRβ signaling resulting from genetic mutations of cytoplasmic signal transduction domains in $Pdgfr\beta^{F7/F7}$ mice (Tallquist *et al*, 2003) leads to gross reductions of spinal cord pericyte populations.

Previous work with pericyte-deficient mice identified three potential mechanisms by which pericytes induce endothelial barrier properties: (1) reduction in vesicular transport and bulk flow transcytosis (Armulik *et al*, 2010; Daneman *et al*, 2010), (2) proper tight junctional alignment (Daneman *et al*, 2010), and (3) promotion of endothelial tight junction expression (Bell *et al*, 2010). Our findings suggest not only

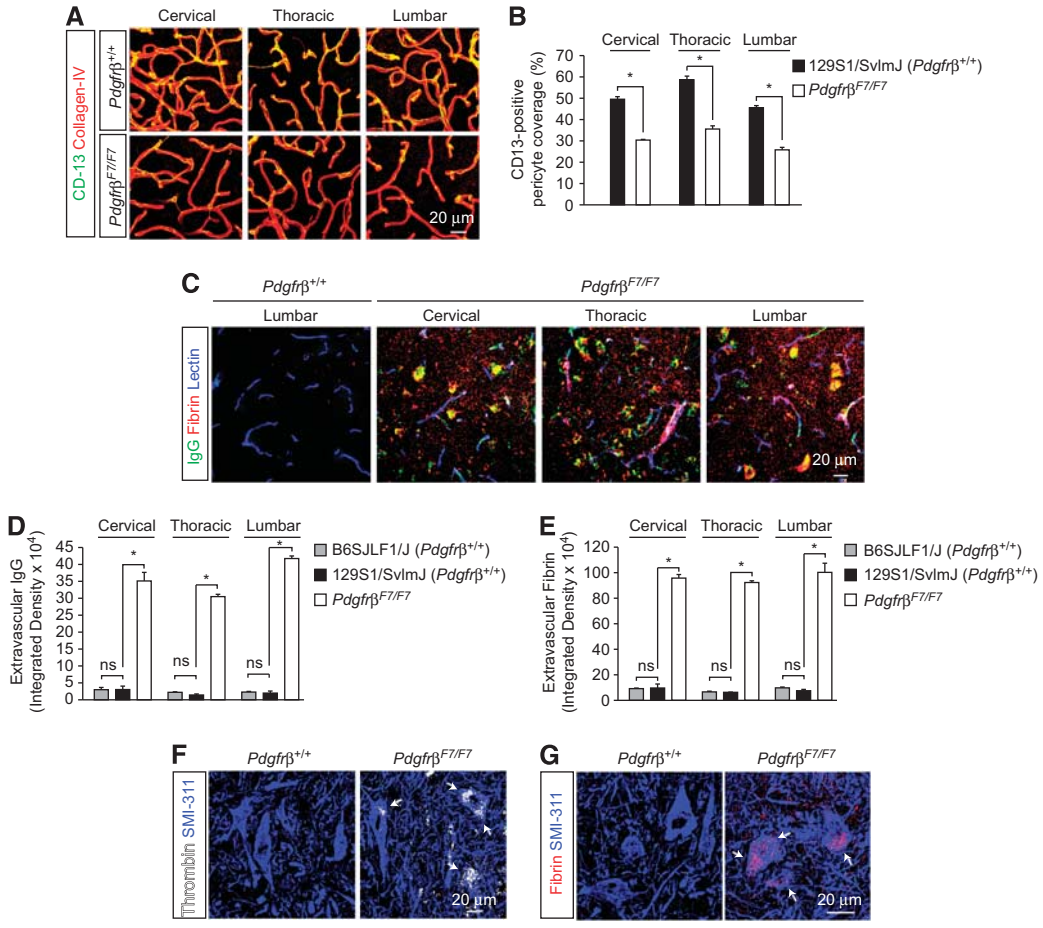

Figure 5 Exacerbation of pericyte deficiency leads to overt blood–spinal cord barrier disruption and leakage of endogenous plasma proteins. (**A**) Confocal microscopy analysis of CD13-positive pericytes (green) and collagen IV-positive capillary profiles (red) in 6-month-old *Pdgfrβ*$^{+/+}$ and *Pdgfrβ*$^{F7/F7}$ mouse cervical, thoracic, and lumbar spinal cord anterior horn. (**B**) Quantification of regional CD13-positive pericyte coverage of collagen IV-positive anterior horn spinal cord capillaries. Mean ± s.e.m., $n = 3$ animals per group; $^*P < 0.05$. (**C**) Representative confocal microscopy analysis of IgG (green), fibrin (red), and lectin-positive capillaries (blue) in 6-month-old *Pdgfrβ*$^{+/+}$ mouse lumbar anterior horn and anterior horn from *Pdgfrβ*$^{F7/F7}$ cervical, thoracic, and lumbar spinal cord. (**D**, **E**) Quantification of IgG (**D**) and fibrin (**E**) extravascular deposits in the spinal cord regions in tissue sections from 2-month-old B6SJL/F1 *Pdgfrβ*$^{+/+}$, 6-month-old *Pdgfrβ*$^{+/+}$ 129S1/SvImJ, and 6-month-old *Pdgfrβ*$^{F7/F7}$ mice. Mean ± s.e.m., $n = 3$ animals per group; $^*P < 0.05$. (**F**, **G**) Confocal microscopy analysis of thrombin (white) (**F**) or fibrin (red) (**G**) and SMI-311-positive neurons (blue) in 6-month-old *Pdgfrβ*$^{+/+}$ and *Pdgfrβ*$^{F7/F7}$ lumbar spinal cord. Arrows indicate neuronal accumulation.

that increased BSCB permeability and regional pericyte reductions in the anterior horn of the spinal cord coincide with reductions in tight junction protein expression (i.e., ZO-1 and occludin), consistent with an increased paracellular flow model. However, further experimental elaboration is required utilizing mouse models in which pericyte deficiency may be rescued to definitely establish a causative relationship between pericytes, endothelial permeability, and the underlying molecular coupling.

Overt vascular barrier disruption in the CNS results in parenchymal accumulation of multiple circulating plasma-derived proteins in neurons (Bell *et al*, 2010; Winkler *et al*, 2011; Zhong *et al*, 2008; Zlokovic, 2011). Many plasma-derived products, including thrombin, fibrin, plasmin and hemoglobin, are neurotoxic and/or vasculotoxic at higher concentrations in the CNS (Bell *et al*, 2010; Chen and Strickland, 1997; Mhatre *et al*, 2004; Paul *et al*, 2007; Zhong *et al*, 2008). In the present report, pericyte reductions in *Pdgfrβ*$^{F7/F7}$ mice correlated with increased BSCB permeability allowing larger toxic plasma proteins such as thrombin (Mhatre *et al*, 2004) and fibrin (Paul *et al*, 2007) to accumulate in motor neurons. In contrast, much less pronounced basal increases in BSCB permeability under physiological conditions in the spinal cord of wild-type mice, that is, a PS product for 40,000 Da dextran in the spinal cord under physiological conditions was nearly 20-fold lower than in *Pdgfrβ*$^{F7/F7}$ mice (Bell *et al*, 2010), did not result in accumulation of larger toxic endogenous macromolecules in motor neurons in either of the nontransgenic mouse strains studied. It is of note, pericytes have been demonstrated to phagocytose

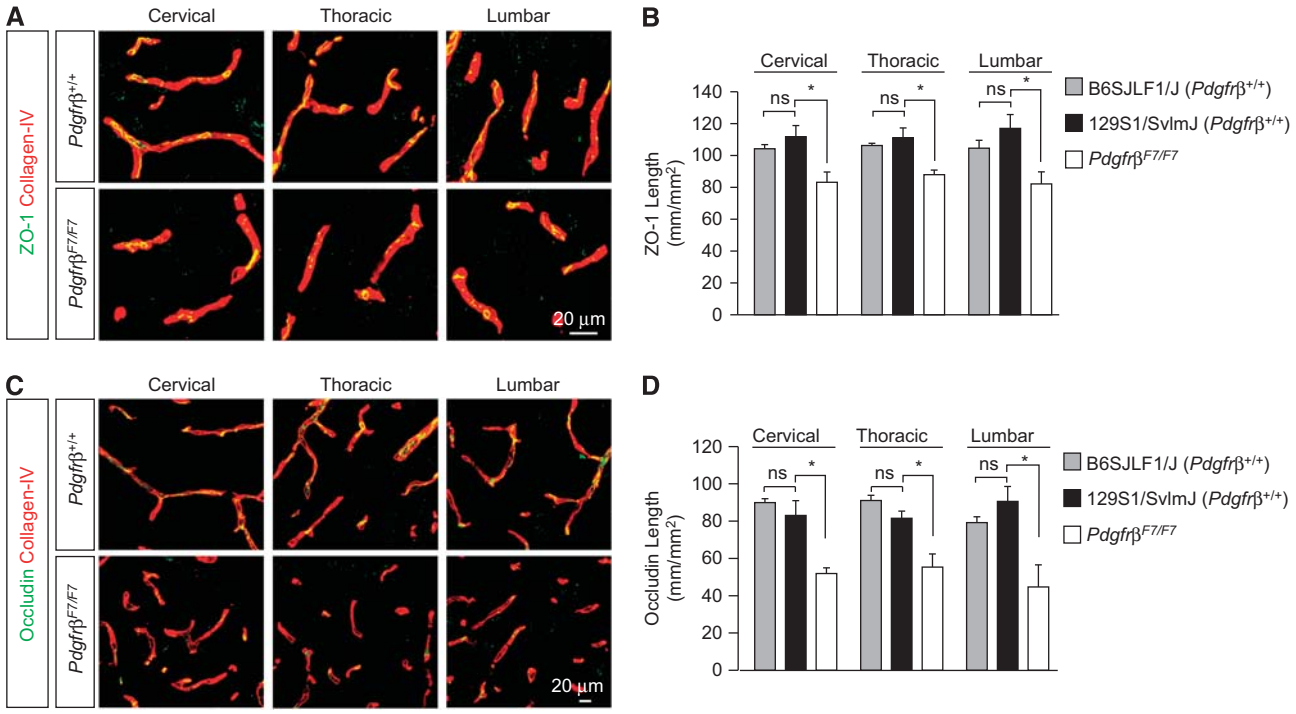

Figure 6 Pericyte deficiency reduces blood–spinal cord barrier (BSCB) tight junction protein expression. (**A**, **C**) Confocal microscopy analysis of tight junction zonula occludens-1 (ZO-1) (**A**) and occludin (**C**) immunodetection (green) in anterior horn from 6-month-old *Pdgfrβ*$^{+/+}$ 129S1/SvImJ and *Pdgfrβ*$^{F7/F7}$ mouse cervical, thoracic, and lumbar spinal cord. (**B**, **D**) Quantification of endothelial ZO-1 (**B**) or occludin (**D**) tight junctional length in spinal cord anterior horn regions in tissue sections from 2-month-old B6SJL/F1 *Pdgfrβ*$^{+/+}$, 6-month-old *Pdgfrβ*$^{+/+}$ 129S1/SvImJ and 6-month-old *Pdgfrβ*$^{F7/F7}$ mice. Mean ± s.e.m. $n = 3$ to 4 preparations per group (five mice per preparation); $^*P < 0.05$.

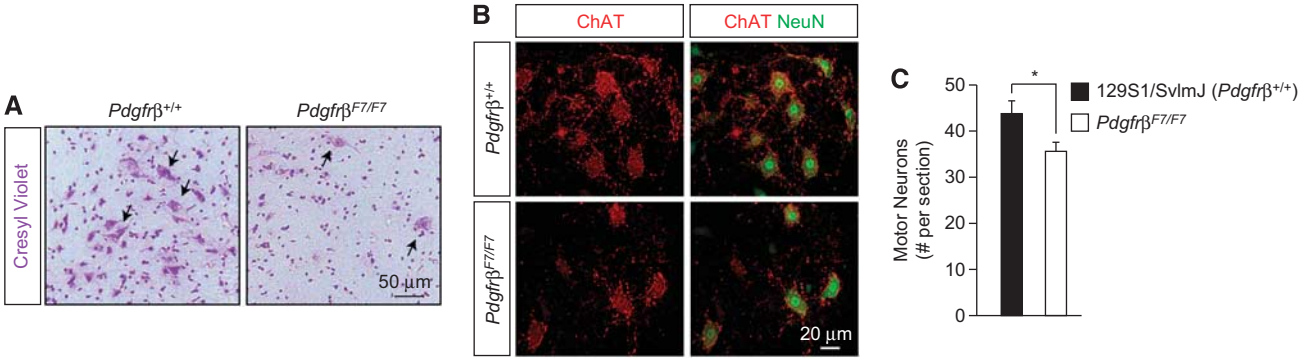

Figure 7 Pericyte deficiency leads to spinal cord structural abnormalities and motor neuron loss. (**A**) Bright-field microscopy analysis of cresyl violet staining (purple) in the lumbar spinal cord anterior horn in a 13-month-old *Pdgfrβ*$^{+/+}$ and *Pdgfrβ*$^{F7/F7}$ mouse. Arrows, cells morphologically consistent with motor neurons. (**B**) Representative confocal microscopy analysis of NeuN-positive (green) and choline acetyl transferase (ChAT)-positive motor neurons (red) in the 13-month-old *Pdgfrβ*$^{+/+}$ and *Pdgfrβ*$^{F7/F7}$ lumbar spinal cord anterior horn. (**C**) Quantification of motor neurons per section in *Pdgfrβ*$^{+/+}$ and *Pdgfrβ*$^{F7/F7}$ lumbar spinal cord anterior horn. Mean ± s.e.m. $n = 3$ mice per group; $^*P < 0.05$.

multiple endogenous proteins and provide an important clearance pathway for extravasated plasma components (Bell *et al*, 2010; Diaz-Flores *et al*, 2009). Therefore, chronic deposition of endogenous plasma-derived proteins in F7 pericyte-deficient mice likely reflect a combination of an increased influx following heightened barrier disruption and reduced pericyte-mediated clearance of these plasma proteins. In contrast, metabolically inert polar exogenous tracers, that is, dextrans, are not taken up by CNS vascular cells *in vitro* (Weksler *et al*, 2005; Zhu *et al*, 2010) or *in vivo* (Bell *et al*, 2010, 2012), and their detection in the CNS following acute injection reflects mainly barrier disruption in isolation of cellular clearance. It is of note, the PS products in the brain regions (e.g., cortex) obtained in B6SJLF1/J mice in the present

study for both 40,000 and 150,000 Da dextran are virtually identical to values obtained in 129S1/SvlmJ wt mice cortices, as we reported (Bell *et al*, 2010), further supporting that changes in BSCB permeability are not strain-specific, but could be molecule-specific.

Blood–spinal cord barrier disruption has been implicated early in multiple spinal cord disease processes including amyotrophic lateral sclerosis (Garbuzova-Davis *et al*, 2011; Zhong *et al*, 2008, 2009), multiple sclerosis, acute spinal cord injury, and several others (Bartanusz *et al*, 2011). Whether BSCB disruption contributes to spinal neurodegenerative changes is not known. Consistent with previous reports in the brain (Bell *et al*, 2010, 2012), our data showing a loss of motor neurons in the lumbar spinal cord suggests that pericyte deficiency and/or breakdown of BSCB may contribute to motor neuron injury. Future studies are needed, however, utilizing inducible models of pericyte deficiency and/or genetic models to rescue pericyte deficiency to better establish the causative relationship between spinal cord microvascular changes and motor neuron injury. At the present time, the mechanisms of motor neuron cell death or whether neuronal dysfunction precedes cellular loss in pericyte-deficient mice are not known and should be addressed in future studies. Proper characterization of spinal cord pericyte populations in human spinal cord diseases may hold considerable promise to better elucidate the interface of vascular dysfunction in spinal cord neurodegeneration.

Disclosure/conflict of interest

The authors declare no conflict of interest.

References

Armulik A, Genove G, Betsholtz C (2011) Pericytes: developmental, physiological, and pathological perspectives, problems, and promises. *Dev Cell* 21:193–215

Armulik A, Genove G, Mae M, Nisancioglu MH, Wallgard E, Niaudet C, He L, Norlin J, Lindblom P, Strittmatter K, Johansson BR, Betsholtz C (2010) Pericytes regulate the blood-brain barrier. *Nature* 468:557–61

Bartanusz V, Jezova D, Alajajian B, Digicaylioglu M (2011) The blood-spinal cord barrier: morphology and clinical implications. *Ann Neurol* 70:194–206

Bell RD, Winkler EA, Sagare A, Singh I, Deane R, Wu Z, Holtzman DM, Betsholtz C, Armulik A, Sallstrom J, Berk B, Zlokovic BV (2012) Apolipoprotein E controls cerebrovascular integrity via cyclophilin A. *Nature* 485: 512–516

Bell RD, Winkler EA, Sagare AP, Singh I, LaRue B, Deane R, Zlokovic BV (2010) Pericytes control key neurovascular functions and neuronal phenotype in the adult brain and during brain aging. *Neuron* 68:409–27

Chen ZL, Strickland S (1997) Neuronal death in the hippocampus is promoted by plasmin-catalyzed degradation of laminin. *Cell* 91:917–25

Daneman R, Zhou L, Kebede AA, Barres BA (2010) Pericytes are required for blood-brain barrier integrity during embryogenesis. *Nature* 468:562–6

Daniel PM, Lam DK, Pratt OE (1985) Comparison of the vascular permeability of the brain and the spinal cord to mannitol and inulin in rats. *J Neurochem* 45:647–9

Diaz-Flores L, Gutierrez R, Madrid JF, Varela H, Valladares F, Acosta E, Martin-Vasallo P, Diaz-Flores Jr L (2009) Pericytes. Morphofunction, interactions and pathology in a quiescent and activated mesenchymal cell niche. *Histo Histopathol* 24:909–69

Enge M, Bjarnegard M, Gerhardt H, Gustafsson E, Kalen M, Asker N, Hammes HP, Shani M, Fassler R, Betsholtz C (2002) Endothelium-specific platelet-derived growth factor-B ablation mimics diabetic retinopathy. *EMBO J* 21:4307–16

Fernandez-Klett F, Offenhauser N, Dirnagl U, Priller J, Lindauer U (2010) Pericytes in capillaries are contractile *in vivo*, but arterioles mediate functional hyperemia in the mouse brain. *Proc Natl Acad Sci USA* 107:22290–5

Garbuzova-Davis S, Rodrigues MC, Hernandez-Ontiveros DG, Louis MK, Willing AE, Borlongan CV, Sanberg PR (2011) Amyotrophic lateral sclerosis: a neurovascular disease. *Brain Res* 1398:113–25

Ge S, Pachter JS (2006) Isolation and culture of microvascular endothelial cells from murine spinal cord. *J Neuroimmunol* 177:209–14

Goritz C, Dias DO, Tomilin N, Barbacid M, Shupliakov O, Frisen J (2011) A pericyte origin of spinal cord scar tissue. *Science* 333:238–42

Hellstrom M, Gerhardt H, Kalen M, Li X, Eriksson U, Wolburg H, Betsholtz C (2001) Lack of pericytes leads to endothelial hyperplasia and abnormal vascular morphogenesis. *J Cell Biol* 153:543–53

Jaarsma D, Teuling E, Haasdijk ED, De Zeeuw CI, Hoogenraad CC (2008) Neuron-specific expression of mutant superoxide dismutase is sufficient to induce amyotrophic lateral sclerosis in transgenic mice. *J Neurosci* 28:2075–88

Kim JH, Yu YS, Kim DH, Kim KW (2009) Recruitment of pericytes and astrocytes is closely related to the formation of tight junction in developing retinal vessels. *J Neurosci Res* 87:653–9

Li F, Lan Y, Wang Y, Wang J, Yang G, Meng F, Han H, Meng A, Yang X (2011) Endothelial Smad4 maintains cerebrovascular integrity by activating N-cadherin through cooperation with Notch. *Dev Cell* 20:291–302

Lindahl P, Johansson BR, Leveen P, Betsholtz C (1997) Pericyte loss and microaneurysm formation in PDGF-B-deficient mice. *Science* 277:242–5

Mackic JB, Weiss MH, Miao W, Kirkman E, Ghiso J, Calero M, Bading J, Frangione B, Zlokovic BV (1998) Cerebrovascular accumulation and increased blood-brain barrier permeability to circulating Alzheimer's amyloid beta peptide in aged squirrel monkey with cerebral amyloid angiopathy. *J Neurochem* 70:210–5

Mann GE, Zlokovic BV, Yudilevich DL (1985) Evidence for a lactate transport system in the sarcolemmal membrane of the perfused rabbit heart: kinetics of unidirectional influx, carrier specificity and effects of glucagon. *Biochim Biophys Acta* 819:241–8

Mhatre M, Nguyen A, Kashani S, Pham T, Adesina A, Grammas P (2004) Thrombin, a mediator of neurotoxicity and memory impairment. *Neurobiol Aging* 25:783–93

Pan W, Banks WA, Kastin AJ (1997*a*) Permeability of the blood-brain and blood-spinal cord barriers to interferons. *J Neuroimmunol* 76:105–11

Pan W, Banks WA, Kastin AJ (1997*b*) Blood-brain barrier permeability to ebiratide and TNF in acute spinal cord injury. *Exp Neurol* 146:367–73

Paul J, Strickland S, Melchor JP (2007) Fibrin deposition accelerates neurovascular damage and neuroinflammation in mouse models of Alzheimer's disease. *J Exp Med* 204:1999–2008

Peppiatt CM, Howarth C, Mobbs P, Attwell D (2006) Bidirectional control of CNS capillary diameter by pericytes. *Nature* 443:700–4

Pfister F, Feng Y, vom Hagen F, Hoffmann S, Molema G, Hillebrands JL, Shani M, Deutsch U, Hammes HP (2008) Pericyte migration: a novel mechanism of pericyte loss in experimental diabetic retinopathy. *Diabetes* 57: 2495–2502

Prockop LD, Naidu KA, Binard JE, Ransohoff J (1995) Selective permeability of [3H]-D-mannitol and [14C]-carboxyl-inulin across the blood-brain barrier and blood-spinal cord barrier in the rabbit. *J Spinal Cord Med* 18:221–6

Tallquist MD, French WJ, Soriano P (2003) Additive effects of PDGF receptor beta signaling pathways in vascular smooth muscle cell development. *PLoS Biol* 1:E52

Weksler BB, Subileau EA, Perriere N, Charneau P, Holloway K, Leveque M, Tricoire-Leignel H, Nicotra A, Bourdoulous S, Turowski P, Male DK, Roux F, Greenwood J, Romero IA, Couraud PO (2005) Blood-brain barrier-specific properties of a human adult brain endothelial cell line. *FASEB J* 19:1872–4

Winkler EA, Bell RD, Zlokovic BV (2010) Pericyte-specific expression of PDGF beta receptor in mouse models with normal and deficient PDGF beta receptor signaling. *Mol Neurodegener* 5:32

Winkler EA, Bell RD, Zlokovic BV (2011) Central nervous system pericytes in health and disease. *Nat Neurosci* 14:1398–405

Zhong Z, Deane R, Ali Z, Parisi M, Shapovalov Y, O'Banion MK, Stojanovic K, Sagare A, Boillee S, Cleveland DW, Zlokovic BV (2008) ALS-causing SOD1 mutants generate vascular changes prior to motor neuron degeneration. *Nat Neurosci* 11:420–2

Zhong Z, Ilieva H, Hallagan L, Bell R, Singh I, Paquette N, Thiyagarajan M, Deane R, Fernandez JA, Lane S, Zlokovic AB, Liu T, Griffin JH, Chow N, Castellino FJ, Stojanovic K, Cleveland DW, Zlokovic BV (2009) Activated protein C therapy slows ALS-like disease in mice by transcriptionally inhibiting SOD1 in motor neurons and microglia cells. *J Clin Invest* 119:3437–49

Zhu D, Wang Y, Singh I, Bell RD, Deane R, Zhong Z, Sagare A, Winkler EA, Zlokovic BV (2010) Protein S controls hypoxic/ischemic blood-brain barrier disruption through the TAM receptor Tyro3 and sphingosine 1-phosphate receptor. *Blood* 115:4963–72

Zlokovic BV, Apuzzo ML (1997) Cellular and molecular neurosurgery: pathways from concept to reality—part I: target disorders and concept approaches to gene therapy of the central nervous system. *Neurosurgery* 40:789–803

Zlokovic BV (2008) The blood-brain barrier in health and chronic neurodegenerative disorders. *Neuron* 57:178–201

Zlokovic BV (2011) Neurovascular pathways to neurodegeneration in Alzheimer's disease and other disorders. *Nat Rev Neurosci* 12:723–38

Zlokovic BV, Jovanovic S, Miao W, Samara S, Verma S, Farrell CL (2000) Differential regulation of leptin transport by the choroid plexus and blood-brain barrier and high affinity transport systems for entry into hypothalamus and across the blood-cerebrospinal fluid barrier. *Endocrinology* 141:1434–41

Zlokovic BV, Mackic JB, Wang L, McComb JG, McDonough A (1993) Differential expression of Na,K-ATPase alpha and beta subunit isoforms at the blood-brain barrier and the choroid plexus. *J Biol Chem* 268:8019–25